2048 *Macromolecules* **2010**, *43*, 2048–2053
DOI: 10.1021/ma902230a

Macromolecules
ARTICLE

# Rheology of Carbon Nanotube Networks During Gelation

**D. T. N. Chen,[†] K. Chen,[†] L. A. Hough,[‡] M. F. Islam,[§] and A. G. Yodh*,[†]**

[†]*Department of Physics and Astronomy, University of Pennsylvania, Philadelphia, Pennsylvania 19104-6396,* [‡]*Complex Fluids Laboratory, Rhodia Inc., Bristol, Pennsylvania 19007, and* [§]*Department of Chemical Engineering and Department of Materials Science and Engineering, Carnegie Mellon University, Pittsburgh, Pennsylvania 15213-3890*

*Received October 7, 2009; Revised Manuscript Received December 10, 2009*

ABSTRACT: We report measurements of gelling rigid rod networks composed of a semidilute dispersion of surfactant-stabilized carbon nanotubes. Microrheology is employed to follow the rheological evolution of the suspension from a semidilute solution of unbonded tubes to a bonded gel network with finite yield stress. The rheological data at various time intervals during gelation is readily collapsed onto a single time-cure superposition master curve. A theoretical model based on the crossing probability of rods confined to finite volumes is developed to account for network elasticity. Model predictions compare well with computer simulation and experiments as a function of nanotube volume fraction[1] and cure time.

## Introduction

Filamentous networks play a crucial role in many biological and materials contexts. In living cells, for example, networks of biopolymers facilitate processes such as cell division and motility. Understanding the macroscopic mechanical properties of such networks, even in vitro, is challenging because of a complex interplay between the flexural rigidity of constituent filaments and interfilament interactions such as cross-linking. To date, the most intensively studied model systems are semiflexible filament networks, such as those composed of F-actin wherein entropic stretching of individual filaments dominates network linear and nonlinear viscoelasticity.[2,3] Rigid rod networks, by contrast, are relatively unexplored and should differ from their semiflexible counterparts as a result of enthalpic effects associated with bending, compression, and interfilament bonding. Carbon nanotube networks present opportunities to explore these latter issues. In addition, interest in carbon nanotube networks has grown as a result of their technological potential in composite materials.[4−6] These applications often depend on network connectivity, thus corroborating the need for a better understanding of network formation in this system class.

In this contribution, we employ a combination of rheological measurements, analytic theory, and computer simulation to investigate network formation in aqueous dispersions of single wall carbon nanotubes (SWNTs). On the experimental side, an aqueous dispersion of SWNTs in surfactant is prepared, and, over time, the SWNTs cross-link because of strong localized van der Waals interactions at contact.[1] As the dispersion ages, clusters of bonded SWNTs form and eventually percolate across the sample, driving its rheological response from that of a Newtonian fluid to a gel. Microrheological measurements were made on this system at various time points along the sol−gel transition. Observation of time-resolved "rigidity percolation" in this system of fixed SWNT volume fraction suggests intertube bonding as the dominant contributor to the elasticity. We demonstrate experimentally that the rheology of SWNTs can be scaled onto a single time-cure superposition master curve, consistent with other gelling systems.[7]

*To whom correspondence should be addressed. E-mail: yodh@physics.upenn.edu.

The time-resolved experiments are closely related to the rheometry of fully cured SWNT gels at varying rod volume fractions $\phi$.[1] The latter work found that the low-frequency elastic modulus ($G'$) exhibited rigidity percolation above a critical volume fraction $\phi^*$ with power law form, that is, $G'(\phi) \approx [(\phi - \phi^*)/\phi^*]^{2.3}$. In the present article, we introduce a microscopic model to understand this behavior. The model accounts for the number of intertube contacts in a static randomly oriented rod network as a function of rod volume fraction, length, and diameter; it is based on the crossing probability of rods in finite volumes. An assumption about the relative contributions to the shear modulus of bonds of varying degrees of connectivity permits derivation of an analytic expression for the scaling of shear modulus with rod volume fraction.

Finally, we extend the static model to account for time-resolved sol−gel dynamics. By incorporating bonding kinetics into the static model, we predict the variation of bonding between rods as a function of gelation time, $t$. The new model provides a marked improvement over empirical power law forms that can be and are often used to describe the data. In contrast with previous simulations[8−10] and rheological measurements[1,11,12] of rigid rod networks, ours is the first study to relate directly the measured elasticity of a rigid rod system to its bond connectivity. Importantly, the work provides predictions about the connectivity of rigid rod networks and, potentially, a means for tailoring the mechanical, electrical, and thermal properties in materials composed of rigid rod networks.

## Experimental Section

**Materials.** Primary experiments were conducted on dispersions of SWNTs made by the HiPCO process (Carbon Nanotechnologies) at volume fraction $\phi = 0.0027$. The nanotubes were purified and suspended in filtered deionized water (Millipore) with NaDDBS surfactant (Sigma Aldrich) following the protocol outlined in ref 13. The ratio of SWNT to NaDDBS was 1:10 by weight. We prepared the dispersion by mechanical agitation for 6 h in a high-frequency bath sonicator (Cole-Palmer model 08849-00). A small amount ($\phi \approx 0.0001$) of fluorescently labeled carboxylated polystyrene spheres (Molecular Probes FluoSpheres) of nominal diameter, $2a = 0.46\ \mu$m, was added to

 Published on Web 02/01/2010 

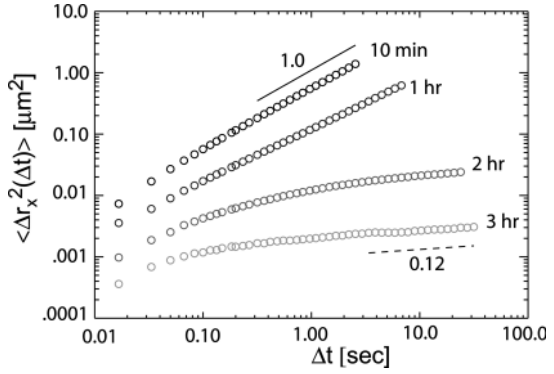


**Figure 1.** Mean square displacement for $2a = 0.46\ \mu$m particles in $\phi =$ 0.27 wt % SWNT, 10:1 NaDDBS/SWNT suspension for $t = 10$ min, 1 h, 2 h, and 3 h (top to bottom). Solid line is slope = 1.0, dashed line is slope = 0.12.

the SWNT-NaDDBS dispersion. The samples were then loaded into a microscope slide and hermetically sealed with optical glue (Norland 63) just prior to each run.

**Methods.** Particle tracking passive microrheology[14,15] was employed to follow the rheological evolution of the network. This method is well suited for measuring viscoelastic moduli of incipient gels because they are generally fragile under shear, and their moduli are often too weak to measure using conventional rheology. The formation of the SWNT bond network was followed by tracking the displacement of ~100 tracer particles in the field of view using digital video microscopy.[16] In typical experiments, 1−5 min of video data were obtained every 30 min over a 4 h period spanning the gelation process. For cure times longer than 3 h, the displacement of the tracers was comparable to the experimental noise, and thus we limited the data presented herein to 3 h or less cure time.

From the tracer trajectories, we compute tracer particle mean square displacement (MSD): $\langle \Delta r_x^2(\Delta t)\rangle = \langle \Delta r_x(t,\Delta t)\Delta r_x(t,\Delta t)\rangle$, where $\Delta r_x(t,\Delta t) = r_x(t+\Delta t) - r_x(t)$ is the particle displacement in the $x$ direction during lag time, $\Delta t$. Note that we calculated two-point MSDs as well[18] and obtained very similar data, but henceforth only one point MSD results will be shown because of its higher statistical resolution at the longest lag times. Owing to the difficulty of imaging through the strongly absorbing SWNT suspension and to minimize sample heating, it was necessary for us to use a relatively long camera shutter time of $\sigma = 1/60$ s on the video CCD camera (Hitachi KP-M1) to achieve adequate signal-to-noise levels in imaging. This led to the introduction of dynamic errors in the MSD, as described in ref 17. We have followed the procedure discussed in ref 17 to correct MSD data for dynamic error. The details of this procedure can be found in the Supporting Information. In the MSD results that follow, the data exhibited are dynamic-error-corrected.

## Results and Discussion

As gelation proceeds, both the magnitude and functional form of the MSD changes. In Figure 1, we exhibit the particle MSD for different waiting times during gelation. For the earliest cure time ($t = 10$ min), the MSD is linear over the entire measurement window, corresponding to a particle diffusing in a Newtonian fluid with viscosity roughly three times larger than that of water. This observation indicates that steric entanglements between unbonded SWNTs do not induce non-Newtonian behavior at this volume fraction. As time progresses, the long lag time behavior of the MSD changes markedly, becoming progressively more subdiffusive at $t = 1$ h and finally exhibiting a nearly flat plateau at $t = 3$ h. Therefore, intertube bonding has progressed to modify the medium's rheological response from purely viscous to strongly elastic.

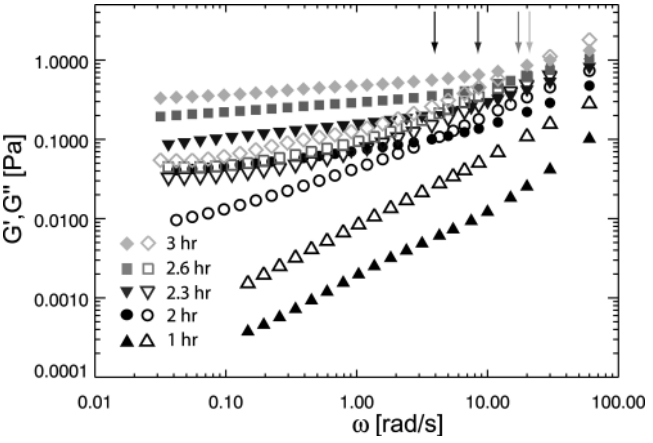


**Figure 2.** Viscoelastic moduli $G'(\omega)$ (closed symbols) and $G''(\omega)$ (open symbols) derived from the MSD. $t > 1.5$ h are in the gel regime ($G' > G''$) data. $t < 1.5$ h are in the sol regime ($G' < G''$) data. Note that in the gel regime, there exists a crossover point [$\omega_c$, $G_c$] where $G'(\omega_c) = G''(\omega_c) = G_c$ indicated by the arrows.

To extract the frequency-dependent (i.e., $\omega$-dependent) viscoelastic moduli, $G^*(\omega)$, from the MSD, we analyze the data using a generalized form of the Stokes−Einstein relation: $G^*(\omega) = k_BT/\pi a i\omega\langle\Delta r^2(\omega)\rangle$, where $\Delta r^2(\omega)$ is the Fourier transform of the MSD. We approximate the transform of the MSD using the numerical approximation scheme detailed in ref 19. The moduli, exhibited in Figure 2, show clear rheological evidence of the sol−gel transition in the SWNT network as a function of gelation time. Below the critical gelation time $1 < t^* < 2$ h, the rheology is dominated by the loss modulus $G''(\omega)$. Above $t^*$, the elastic modulus $G'(\omega)$ dominates at low frequency. For all gelation times in our data, $G'(\omega)$ exhibits a weak frequency dependence ($\sim\omega^{0.3}$) characteristic of soft ($G' \approx 1$ Pa) physical gels and of chemical gels of unbalanced stoichiometry.[20] (Note that we expect for strong gels ($G' \geq 100$ Pa) that $G'(f = \omega/2\omega = 1\ \text{Hz}) = G'(f \rightarrow 0) = G_0'$, where $G_0'$ is the plateau modulus.)

For times longer than $t^*$, the moduli exhibit a point of crossover at which the viscous and elastic components are equal. This defines a crossover modulus, $G_c$, and crossover frequency, $\omega_c$, both of which increase with the gelation time above $t^*$. By scaling the magnitude of $G$ by $G_c$ and the frequency $\omega$ by $\omega_c$, we find that the network moduli exhibit a striking collapse. The main plot of Figure 3 shows the data collapse under time-cure superposition.[21,22] The resulting master curve reveals the viscoelastic relaxation of the NT gel over four decades in frequency. We can collapse the data from different NT concentrations and surfactant ratios onto the same master curve.[23]

We parametrize the extent of the gelation via the dimensionless time parameter $\varepsilon = |t - t^*|/t^*$. Above the gel point, a zero-frequency finite elastic modulus appears and increases as a power law with $\varepsilon$. Experimentally, we find $G_c \approx \varepsilon^z$, where $z \approx 1.03$ (Figure 3, upper inset). For all gelation times in our data, $\omega_c$ is comparable to $\omega \equiv 2\pi f \approx 6.3$ rad/s (Figure 3, lower inset); therefore, $G_c$ and, indeed, the low-frequency elastic modulus $G'(t, f = 1\ \text{Hz})$ exhibit very similar scaling with gelation extent.

In any gelling network wherein both $\omega_c$ and $G_c$ scale as power laws with the cure time (insets of Figure 3), the viscoelastic moduli should be of similar functional form and should collapse under rescaling. Intuitively, $\omega_c$ is related to the mean relaxation time of the bonded rod clusters and $G_c$ is related to their mean elastic modulus, both of which scale with the size of the bonded clusters. Therefore, the effect of an increase in the number of bonds corresponds, essentially, to a rescaling of time in the curing gel. As gelation proceeds ($t > t^*$), the bonds percolate, producing a change in connectivity without reorganization of the network

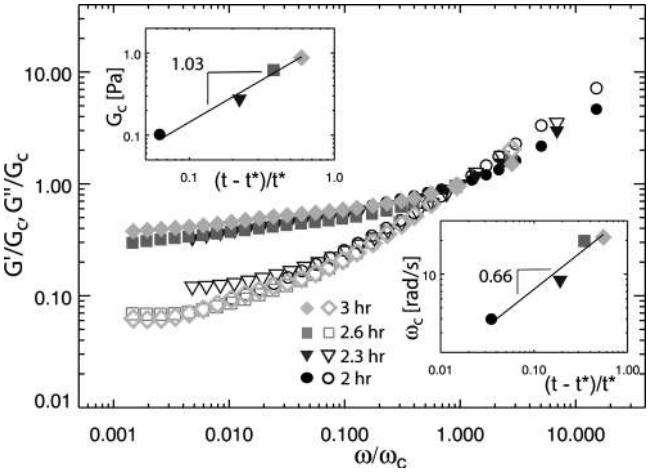


**Figure 3.** Collapsed rheological master curve obtained by scaling $G'(\omega)$ (closed symbols) and $G''(\omega)$ (open symbols) by their respective crossover frequency $\omega_c$ and modulus $G_c$. Upper inset: $G_c$ versus gelation extent, scaling as $G_c \approx [(t - t^*)/t^*]^{1.03}$ with $t^* = 6777$ s. Lower inset: $\omega_c$ versus gelation extent, scaling as $\omega_c \approx [(t - t^*)/t^*]^{0.66}$ with $t^* = 6957$ s.

structure. The collapse of the viscoelastic moduli for the curing SWNT network under time-cure superposition highlights the crucial role of bonding between rods, which we explicate further below.

## Theory Section

Clearly, bonding between rods is the dominant contributor to the elasticity in the gel because the number of rods is constant in time and $G'$ increases with time. Here we introduce a microscopic theory that establishes the relationship between elastic modulus $G'$ and number of contacts, $N_c$, in the system, first for static and then dynamic networks. The first part of the theory derives, from the crossing probability of rods, a relation defining the number of contacts for a given density of randomly oriented rods. We then derive a relation for the shear modulus given an effective number of contacts, which is a fraction of all contacts. These results are corroborated with computer simulations and are used to fit both static[1] and dynamic experimental rheology data.

**Static Model.** The crossing probability of randomly oriented rods confined to a finite volume has an expected number of contacts, $N_c$, which purely depends on geometric parameters. A simple calculation yields an expression for the number density of contacts. (See the Supporting Information for full details of calculation.)

$$\frac{N_c}{V} = C\frac{L^2\sigma N_{rod}^2}{V^2} \approx \phi^2 \qquad (1)$$

Here $\phi = (\pi N_{rod} L\sigma^2)/4V$ is the volume fraction of rods, and rod diameter, $\sigma$, is assumed to be constant. Equation 1 predicts the number of contacts in a randomly oriented network of rods as a function of the number of rods, $N_{rod}$, rod length, $L$, and rod diameter, $\sigma$. (Note that similar $L^2\sigma$ scaling is found in the excluded volume analysis of percolation at large rod aspect ratios.[24]) The volume of the sample space is $V$.

Because we cannot directly observe the bonding between nanoscale rods in solution, computer simulations are employed to test the predictions of this theory. We construct static networks of monodisperse rods of length, $L = 10$, diameter, $\sigma = 0.05$, and aspect ratio, $L/\sigma = 200$, chosen to be comparable to the SWNTs in our experiments. (Note that the SWNTs used in the experiments are polydisperse in length. We also carried out simulations for rods with lengths drawn from a Gaussian distribution of comparable polydispersity to the SWNTs used in the experiments; a significant deviation of $N_c/V$ from the results for monodisperse rods was not found.) The results that follow are from simulations of monodisperse rods.

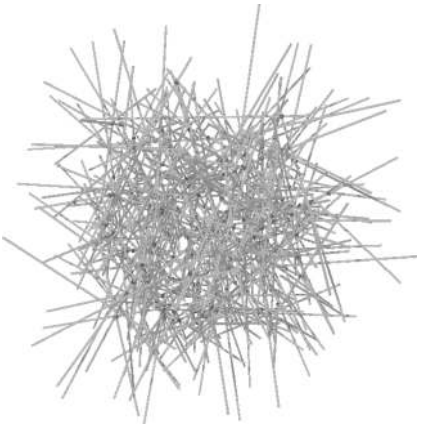

**Figure 4.** Snapshot of simulation for $N = 100$ rods of aspect ratio $L/\sigma = 200$ confined to a volume $V = 10^3$. Spheres indicate contacts between rods.

**Simulations.** Rods are deposited randomly (off-lattice) in a 3D periodic cube with linear dimension $\ell = 20-40$. Then, we determine whether the randomly deposited rod central axes approach one another within a prescribed distance. Physically, we choose this distance to be the rod diameter. A contact is said to form between two rods when the distance between their points of closest separation is less than or equal to the rod diameter. Note that this definition for contact permits rods to interpenetrate (i.e., soft core). A snapshot taken from a simulation is given in Figure 4, where dark spheres mark the points of intersection between rods located by the algorithm.

To test the scaling prediction of eq 1, we varied the sample volume ($V$ ranged from $20^3$ to $40^3$) and rod length ($L$ ranged from 5 to 10) while keeping rod diameter constant ($\sigma = 0.05$) in the simulations. In Figure 5A, we plot the number of contacts, $N_c$, versus the total number of rods, $N_{rod}$, in our simulations. Rescaling the $N_c$ by $V/L^2$ in accordance with eq 1 yields a collapse of the data, as shown in Figure 5B. This collapse validates the first piece of our theoretical model for the crossing probability of rigid rods. We next extend the model in two successive steps: first, we derive the macroscopic shear modulus from consideration of only elastically effective bonds, and, second, we derive the temporal evolution of elasticity assuming first-order bonding kinetics.

Some bonds do not contribute to the shear modulus of the network; for example, some rods will have only a single bond, and these noncontributing bonds need to be excluded when the shear modulus is computed. Physically, these bonds are akin to "dangling" strands in polymer melts.[25] In Figure 6B, we illustrate two types of bonds that occur in a cluster of rods. The bonds denoted by circles belong to a pair of rods that are both connected to other rods, that is, multiply connected bonds. The bonds denoted by stars belong to a pair of rods for which one of the rods is not connected to any other rods, that is, singly connected bonds. Physically, we expect only the multiply connected bonds to respond elastically under shear and thus to contribute to the measured shear modulus in a rheology measurement, as depicted in Figure 6D. We define an exclusion probability $P_{exc} = N_s/N_c$, where $N_s$ is the number of noncontributing

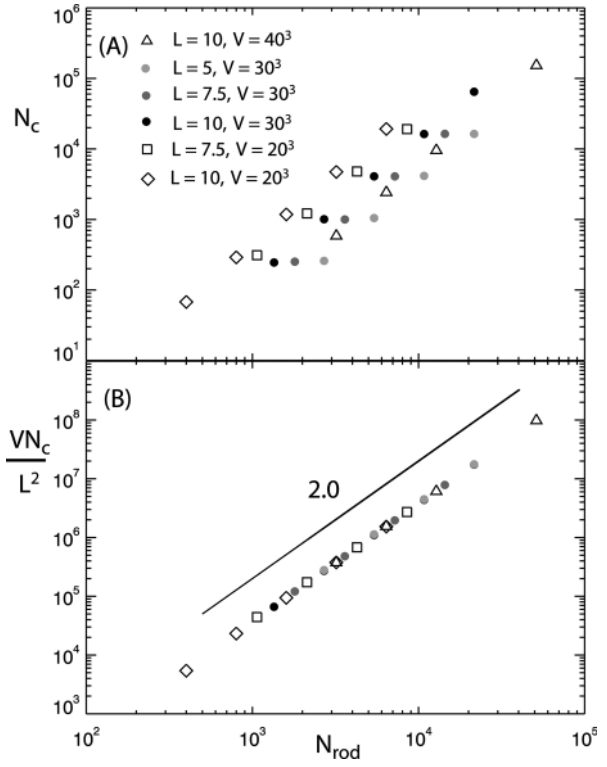


**Figure 5.** (A) Number of contacts versus number of rods in the simulation box. Data shown are for different box volumes and rod lengths. (B) Data collapse under rescaling of contact number by $V/L^2$. Solid line is slope 2.0.

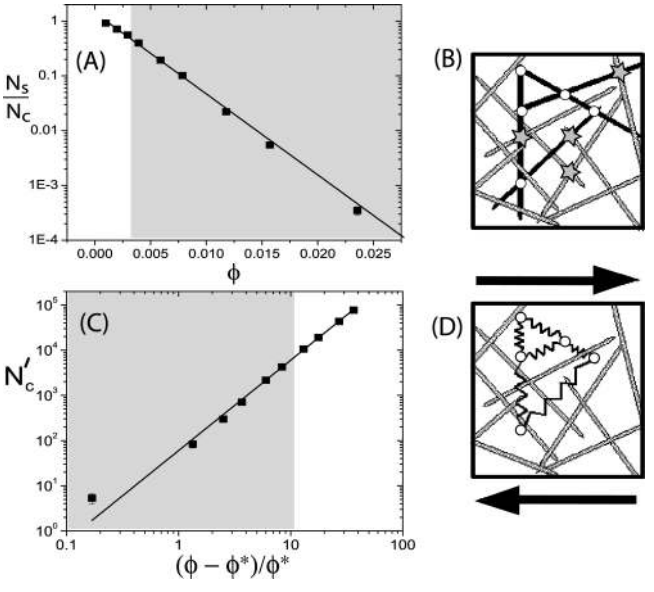


**Figure 6.** (A) Ratio of number of single bonds to number of total contacts ($N_s/N_c$) versus volume fraction from simulation. Solid line is fit to $e^{-B(\phi-\phi^*)/\phi^*}$ with $\phi^* = (1.0 \pm 0.1) \times 10^{-3}$ and $B = 0.345 \pm 0.036$. Shaded region corresponds to concentration regime of rheology data in Figure 7. (B) Cartoon of rod network showing multiply connected bonds (circles) and single bonds (stars). Multiply connected rods are black. (C) Number of contacts with single bonds removed ($N'_c = N_c - N_s$) versus $(\phi - \phi^*)/\phi^*$ from simulation. Solid line is fit to eq 2 (see the text) with $A = (781.5 \pm 2.2) \times 10^5$, $\phi^* = (8.35 \pm 1.46) \times 10^{-4}$, and $B = 0.253 \pm 0.063$. (D) Cartoon illustrating that only the nonsingle bonds contribute to an elastic response under shear.

bonds. When the volume fraction is low, almost all bonds are noncontributing bonds. The exclusion probability decreases

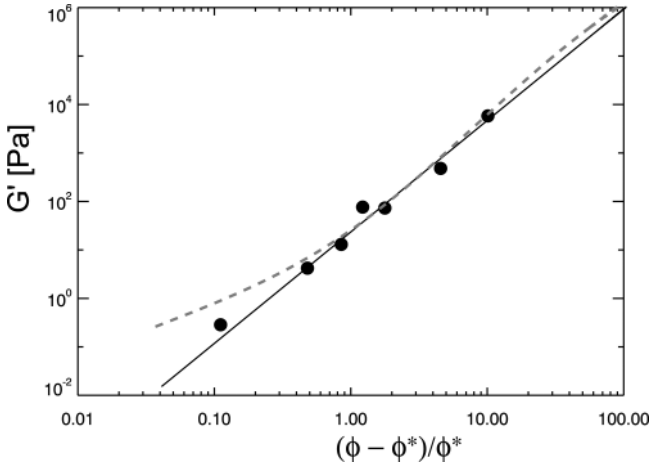


**Figure 7.** Low-frequency elastic modulus $G'(f = 1$ Hz) versus volume fraction from rheology. Data is taken from ref 1. Dashed line is fit to eq 2 with $\phi^* = 0.0028 \pm 0.0001$ and $B = 0.053 \pm 0.007$. Solid line is fit to critical power law $A[(\phi - \phi^*)/\phi^*]^\beta$ with $\phi^* = 0.0027 \pm 0.0002$ and $\beta = 2.3 \pm 0.1$.

as the packing fraction increases because it is progressively more difficult for a rod or a cluster of rods to be isolated from the rest of the sample. We extract the volume fraction dependence of the $P_{exc}$ from a simulated network with $V = 20^3$, $L = 10$, and $\sigma = 0.05$. The results, exhibited in Figure 6A, show that the exclusion probability is well approximated by an exponential function: $P_{exc} = e^{-B(\phi-\phi^*)/\phi^*}$, where $\phi^*$ is the volume fraction at which the sample starts to develop a shear modulus and $B$ is a dimensionless parameter characterizing the rate of decrease in noncontributing bonds with increasing $\phi$. Note that this theoretical form is one of several possible functions; here we chose a natural form with a minimum number of free parameters.

Therefore, the density of bonds that contribute to the sample shear modulus is

$$\frac{N'_c}{V} = \frac{N_c}{V}(1 - P_{exc}) = A\phi^2(1 - e^{-B(\phi-\phi^*/\phi^*)}) \qquad (2)$$

where $A$ is a constant of proportionality. The number of elastically effective contacts ($N'_c$) is given by the total number of contacts minus the number of single bonds (i.e., $N'_c = N_c - N_s$). From the simulation data of Figure 6A, we obtain the number of effective contacts and plot it versus the volume fraction of rods. The results, exhibited in Figure 6C, show that $N'_c$ is well fit by eq 2.

## Comparison with Rheology Experiments

Our previous rheological measurements yielded a scaling of the low frequency elastic modulus $G'(\phi, f = 1$ Hz) with rod volume fraction that was well described by the critical power law form $A[(\phi - \phi^*)/\phi^*]^\beta$ with $\phi^* = 0.0027 \pm 0.0002$ and $\beta = 2.3 \pm 0.1$.[1] It is worth noting that the simple power law $A\phi^2$ does not fit the rheology data at all, confirming that the data are in a regime (indicated in the shaded areas of Figure 6A,C), where we expect a relatively high fraction of single bonds to have a significant effect on the measured shear modulus. It follows that if $G' \approx N'_c$, then eq 2 should also fit the volume-fraction-dependent $G'$ rheological data with only a different constant of proportionality. Indeed, as Figure 7 attests, we find comparable fit quality when comparing eq 2 against $A[(\phi - \phi^*)/\phi^*]^\beta$ for the rheological data of ref 1. Note that both expressions have three free parameters. Whereas the critical power law form is more commonly used to fit scaling data

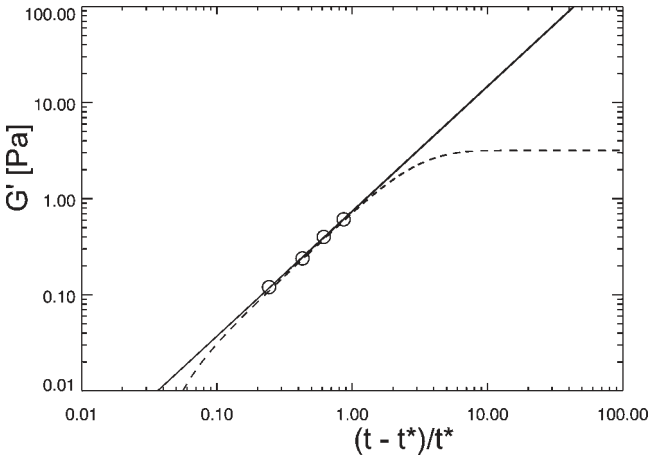


**Figure 8.** Low-frequency elastic modulus $G'(f = 1Hz)$ versus cure time from microrheology. Dashed line is fit to eq 4 with $\phi = 0.006 \pm 0.001$, $\gamma = 0.0175 \pm 0.007$, $\phi^* = 0.0028$, and $B = 0.053$. Solid line is fit to power law $A((t - t^*)/t^*)^z$ with $t^* = 5793 \pm 479$ s and $z = 1.3 \pm 0.2$.

for gelation, it is largely empirical. Equation 2, on the other hand, has been derived from the crossing probability of rods in a confined geometry, augmented with minimal assumptions about the relative contribution to the shear modulus from bonds with differing degrees of connectivity. The discrepancy between the values of $\phi$ and $B$ obtained from fitting eq 2 to simulations ($\phi^* = 8.35 \pm 1.46) \times 10^{-4}$, $B = 0.253 \pm 0.068$) and experiments ($\phi^* = 0.0028 \pm 0.0001$, $B = 0.053 \pm 0.007$) is likely due to the fact that our model does not exclude the bonds in higher-order structures such as nonspanning clusters and dangling closed loops. In a real network, these structures will not contribute to elasticity, resulting in a higher value for $\phi^*$, consistent with our fitted values for $\phi^*$. Instead, we have focused on excluding the simplest structures (single bonds), which, while sidestepping complicated considerations such as finite-size effects, may have come at the expense of exact quantitative agreement between $\phi^*$ and $B$ between the simulations and experiments.

## Comparison with Microrheology Experiments

To compare with the dynamic results from the present microrheology experiments, we extend our theoretical model for static rod networks to account for the time evolution of rod bonding in an adequately dispersed sample. At any given time, $N_f$ free rods are not bonded to any other rods, and $N_b$ rods are bonded $N_f + N_b = N_{tot}$. At $t = 0$, we take $N_f = N_{tot}$ and $N_b = 0$. Conversely, at $t = \infty$, we take $N_b = N_{tot}$ and $N_f = 0$. The rate of bonding is proportional to the number of free rods that are actively seeking bonds and to the total number of rods that are candidates for additional bonding. Accordingly, the time dependence of bond formation is given by the rate equation $dN_f/dt = -\gamma N_f N_{tot}$, where $\gamma$ is the bonding rate. Integrating the rate equation and applying boundary conditions yields the number of bonded rods as a function of time

$$N_b = N_{tot}(1 - e^{-\gamma N_{tot} t}) \quad (3)$$

Substituting $N_b$ for $N_{rod}$ in the static analysis of eqs 1 and 2 yields the time evolution of the low-frequency elastic modulus

$$G' = A\phi^2(1 - e^{-\gamma\phi t})^2[1 - e^{-B(\phi(1 - e^{-\gamma\phi t}) - \phi^*/\phi^*)}] \quad (4)$$

Equation 4 suggests that $G'$ will eventually saturate (i.e., $G' \rightarrow A\phi^2$ as $t \rightarrow \infty$) when all possible bonding rods are exhausted. The elastic modulus $G'(t, f = 1$ Hz) for different cure times, shown in Figure 8 can be fit by a power law form $A[(t - t^*)/t^*]^z$ with $z = 1.3 \pm 0.2$. This is not surprising because the sample is rather dilute, and the time it takes for $G'$ to saturate lies outside our experimental window. Physically, however, $G'$ must saturate on approach to its fully cured value, corresponding to the modulus at which all available rods are bonded. Clearly, this saturation behavior is not captured in the power law, which grows indefinitely ($G' \rightarrow A(t/t^*)^z$ as $t \rightarrow \infty$). Therefore, the power law is at best an empirical local approximation to a saturating functional form. We can fit the microrheology data equally well to either eq 4 or the power law $A[(t - t^*)/t^*]^z$, as shown in Figure 8, because of the limited dynamic range of the data. In fitting eq 4, we have fixed $\phi^* = 0.0028$ and $B = 0.053$, the values extracted from the rheology data fitting of Figure 7. As a result, both functional forms have three parameters. In principle, we could have further constrained $\phi$ in eq 4. However, to account for modulus variations between the two data sets due to sample preparation, it was necessary to let $\phi$ vary. Nonetheless, the nearly indistinguishable fitting over the dynamic range of our data suggests that its time dependence is well captured by our model. Measurements for longer cure times are clearly needed to test conclusively eq 4.

## Conclusions

We have performed microrheological measurements of the gelation of a semidilute suspension of single-wall carbon nanotubes. The results implicate intertube bonding as the dominant contributor to elasticity in the system. To elucidate the quantitative dependence of the number of bonds on geometric parameters characterizing the rods, we have derived an expression, based on the crossing probability of rods confined to a finite volume, that yields the dependence of the number of contacts on the density, length, and diameter of the constituent rods. The relation is shown to be in agreement with the scaling of the number of contacts for simulated rigid rod networks. To make connection with the shear modulus measured in rheology experiments, we have assumed that only the fraction of bonds belonging to multiply connected rods contributes to the network's elasticity. With this assumption, we derived a relation that fits the static macro- and dynamic microrheological data with a goodness-of-fit comparable to empirically derived critical power laws. Future rheological measurements or detailed finite element simulations with larger dynamic range are needed to test decisively the models.

**Acknowledgment.** We acknowledge stimulating discussions with Mateusz Bryning, Andy Lau, Tom Lubensky, and Brian DiDonna. This work has been partially supported by the NSF MRSEC (DMR-0505048 and DMR 05-20020) and NASA (NAG-2939).

**Supporting Information Available:** Detailed discussion of dynamic error correction procedure for the MSD data. Detailed derivation of eq 1 in the main text. This material is available free of charge via the Internet at http://pubs.acs.org.

## References and Notes

(1) Hough, L. A.; Islam, M. F.; Janmey, P. A.; Yodh, A. G. *Phys. Rev. Lett.* **2004**, *93*, 168102.
(2) Gardel, M. L.; Shin, J. H.; MacKintosh, F. C.; Mahadevan, L.; Matsudaira, P.; Weitz, D. A. *Science* **2004**, *304*, 1301–1305.
(3) Storm, C.; Pastore, J. J.; MacKintosh, F. C.; Lubensky, T. C.; Janmey, P. A. *Nature* **2005**, *435*, 191–194.
(4) Geng, H. Z.; Rosen, R.; Zheng, B.; Shimoda, H.; Fleming, L.; Liu, J.; Zhou, O. *Adv. Mater.* **2002**, *14*, 1387–1390.
(5) Huang, Y. Y.; Ahir, S. V.; Terentjev, E. M. *Phys. Rev. B* **2006**, *73*, 125422.

(6) Moniruzzaman, M.; Winey, K. I. *Macromolecules* **2006**, *39*, 5194–5205.
(7) Larsen, T. H.; Furst, E. M. *Phys. Rev. Lett.* **2008**, *100*, 146001.
(8) Wilhelm, J.; Frey, E. *Phys. Rev. Lett.* **2003**, *91*, 108103.
(9) DiDonna, B. A.; Morse, D. C. arXiv: cond-mat/0703418v1.
(10) Foygel, M.; Morris, R. D.; Anez, D.; French, S.; Sobolev, V. L. *Phys. Rev. B* **2005**, *71*, 104201.
(11) Hobbie, E. K.; Fry, D. J. *J. Chem. Phys.* **2007**, *126*, 124907.
(12) Lin, Y. C.; Koenderink, G. H.; MacKintosh, F. C.; Weitz, D. A. *Macromolecules* **2007**, *40*, 7714–7720.
(13) Islam, M. F.; Rojas, E.; Bergey, D. M.; Johnson, A. T.; Yodh, A. G. *Nano Lett.* **2003**, *3*, 269–273.
(14) Mason, T. G.; Ganesan, K.; van Zanten, J. H.; Wirtz, D.; Kuo, S. C. *Phys. Rev. Lett.* **1997**, *79*, 3282–3285.
(15) Chen, D. T.; Weeks, E. R.; Crocker, J. C.; Islam, M. F.; Verma, R.; Gruber, J.; Levine, A. J.; Lubensky, T. C.; Yodh, A. G. *Phys. Rev. Lett.* **2003**, *90*, 108301.
(16) Crocker, J. C.; Grier, D. G. *J. Colloid Interface Sci.* **1996**, *179*, 298–310.
(17) Savin, T.; Doyle, P. S. *Biophys. J.* **2005**, *88*, 623–638.
(18) Crocker, J. C.; Valentine, M. T.; Weeks, E. R.; Gisler, T.; Kaplan, P. D.; Yodh, A. G.; Weitz, D. A. *Phys. Rev. Lett.* **2000**, *85*, 888–891.
(19) Dasgupta, B. R.; Tee, S. Y.; Crocker, J. C.; Frisken, B. J.; Weitz, D. A. *Phys. Rev. E* **2002**, *65*, 051505.
(20) Curro, J. G.; Pincus, P. *Macromolecules* **1983**, *16*, 559–562.
(21) Adolf, D.; Martin, J. E. *Macromolecules* **1990**, *23*, 3700–3704.
(22) Winter, H. H.; Chambon, F. *J. Rheol.* **1986**, *30*, 367–382.
(23) Chen, D. T. N. Ph.D. Thesis, University of Pennsylvania, Philadelphia, PA, 2010.
(24) Balberg, I.; Anderson, C. H.; Alexander, S.; Wagner, N. *Phys. Rev. B.* **1984**, *30*, 3933–3943.
(25) deGennes, P. G. *Scaling Concepts in Polymer Physics*; Cornell University Press: Ithaca, NY, 1990.